Publication Year	2020
Acceptance in OA	2022-01-21T14:42:35Z
Title	Alignment of the optical system of the 9.7-m prototype Schwarzchild-Coulder Telescope
Authors	Adams, C., Alfaro, R., Ambrosi, G., Ambrosio, M., Aramo, C., Benbow, W., Bertucci, B., Bissaldi, E., Bitossi, M., Boiano, A., Bonavolontá, C., Bose, R., Brill, A., Buckley, J. H., Byrum, K., Cameron, R. A., Capasso, M., Caprai, M., Covault, C. E., Di Venere, L., Fegan, S., Feng, Q., Fiandrini, E., Furniss, A., Garczarczyk, M., Garfias, F., Gent, A., Giglietto, N., Giordano, F., González, M. M., Halliday, R., Humensky, T. B., Ribeiro, D., Hervet, O., Hughes, G., Ionica, M., Iriarte, A., Jin, W., Kaaret, P., Kieda, D., Kim, B., Limon, M., Loporchio, S., Meures, T., Mode, B. A. W., Mukherjee, R., Nieto, D., Okumura, A., Otte, N., LA PALOMBARA, NICOLA, Pantaleo, F. R., Paoletti, R., PARESCHI, Giovanni, Petrashyk, A., Powell, J., Roache, E., Rousselle, J., Rugliancich, A., Ruíz-Díaz-Soto, J., Santander, M., Schlenstedt, S., SCUDERI, Salvatore, Shang, R., SIRONI, GIORGIA, Stevenson, B., Stiaccini, L., Taylor, L. P., Tosti, L., Tovmassian, G., Vagelli, V., Valentino, M., Vandenbroucke, J., Vassiliev, V., Wakely, S. P., Wilcox, P., Williams, D. A., Yu, P.
Publisher's version (DOI)	10.1117/12.2564653
Handle	http://hdl.handle.net/20.500.12386/31339
Serie	PROCEEDINGS OF SPIE
Volume	11445

Alignment of the optical system of the 9.7-m prototype Schwarzchild-Coulder Telescope

Adams, C., Alfaro, R., Ambrosi, G., Ambrosio, M., Aramo, C., et al.

C. Adams, R. Alfaro, G. Ambrosi, M. Ambrosio, C. Aramo, W. Benbow, B. Bertucci, E. Bissaldi, M. Bitossi, A. Boiano, C. Bonavolontá, R. Bose, A. Brill, J. H. Buckley, K. Byrum, R. A. Cameron, M. Capasso, M. Caprai, C. E. Covault, L. Di Venere, S. Fegan, Q. Feng, E. Fiandrini, A. Furniss, M. Garczarczyk, F. Garfias, A. Gent, N. Giglietto, F. Giordano, M. M. González, R. Halliday, T. B. Humensky, D. Ribeiro, O. Hervet, G. Hughes, M. Ionica, A. Iriarte, W. Jin, P. Kaaret, D. Kieda, B. Kim, M. Limon, S. Loporchio, T. Meures, B. A. W. Mode, R. Mukherjee, D. Nieto, A. Okumura, N. Otte, N. La Palombara, F. R. Pantaleo, R. Paoletti, G. Pareschi, A. Petrashyk, J. Powell, E. Roache, J. Rousselle, A. Rugliancich, J. Ruíz-Díaz-Soto, M. Santander, S. Schlenstedt, S. Scuderi, R. Shang, G. Sironi, B. Stevenson, L. Stiaccini, L. P. Taylor, L. Tosti, G. Tovmassian, V. Vagelli, M. Valentino, J. Vandenbroucke, V. Vassiliev, S. P. Wakely, P. Wilcox, D. A. Williams, P. Yu, "Alignment of the optical system of the 9.7-m prototype Schwarzchild-Coulder Telescope," Proc. SPIE 11445, Ground-based and Airborne Telescopes VIII, 114456A (14 December 2020); doi: 10.1117/12.2564653

SPIE.

Event: SPIE Astronomical Telescopes + Instrumentation, 2020, Online Only

Alignment of the Optical System of the 9.7-m Prototype Schwarzschild-Couder Telescope

C. Adams[a], R. Alfaro[b], G. Ambrosi[c], M. Ambrosio[d], C. Aramo[d], W. Benbow[e], B. Bertucci[c,f], E. Bissaldi[g,h], M. Bitossi[h], A. Boiano[d], C. Bonavolontà[d], R. Bose[i], A. Brill[a], J. H. Buckley[i], K. Byrum[j], R. A. Cameron[k], M. Capasso[n], M. Caprai[c], C. E. Covault[l], L. Di Venere[h], S. Fegan[m], Q. Feng[n], E. Fiandrini[c,f], A. Furniss[o], M. Garczarczyk[p], F. Garfias[q], A. Gent[r], N. Giglietto[g,h], F. Giordano[g,h], M. M. González[q], R. Halliday[l], O. Hervet[s], G. Hughes[t,u], T. B. Humensky[a], M. Ionica[c], A. Iriarte[q], W. Jin[v], P. Kaaret[w], D. Kieda[x], B. Kim[y], F. Licciulli[h], M. Limon[z], S. Loporchio[g,h], V. Masone[d], T. Meures[aa], B. A. W. Mode[aa], R. Mukherjee[n], D. Nieto[ab], A. Okumura[ac], N. Otte[r], N. La Palombara[ad], F. R. Pantaleo[g,h], R. Paoletti[ai,ae], G. Pareschi[af], A. Petrashyk[ag], J. Powell[v], K. Powell[r], D. Ribeiro[a], E. Roache[t], J. Rousselle[ah], A. Rugliancich[ai], J. Ruíz-Díaz-Soto[q], M. Santander[v], S. Schlenstedt[p,u], S. Scuderi[ad], R. Shang[y], G. Sironi[af], B. Stevenson[y], L. Stiaccini[ai,ae], L. P. Taylor[aa], L. Tosti[c,f], G. Tovmassian[q], V. Vagelli[c,aj], M. Valentino[ak,d], J. Vandenbroucke[aa], V. V. Vassiliev[†y], S. P. Wakely[al], P. Wilcox[am], D. A. Williams[s], P. Yu[y], for the CTA SCT Project

[a]Physics Department, Columbia University, New York, NY 10027, USA
[b]Instituto de Física, Universidad Nacional Autónoma de México, Ciudad de Mexico, Mexico
[c]INFN Sezione di Perugia, Perugia, Italy
[d]INFN Napoli, Italy
[e]Center for Astrophysics — Harvard & Smithsonian, Cambridge, MA 02138, USA
[f]Università degli Studi di Perugia, Perugia, Italy
[g]Dipartimento Interateneo di Fisica dell'Università e del Politecnico di Bari
[h]INFN Bari, Via E. Orabona 4, 70125 Bari, Italy
[i]Department of Physics, Washington University, St. Louis, MO 63130, USA
[j]Argonne National Laboratory, 9700 S. Cass Avenue, Argonne, IL 60439, USA
[k]Kavli Institute for Particle Astrophysics and Cosmology, SLAC National Accelerator Laboratory, Stanford University, Stanford, CA 94305, USA
[l]Department of Physics, Case Western Reserve University, Cleveland, Ohio 44106, USA
[m]LLR/Ecole Polytechnique, Route de Saclay, 91128 Palaiseau Cedex, France
[n]Department of Physics and Astronomy, Barnard College, Columbia University, NY 10027, USA
[o]Department of Physics, California State University - East Bay, Hayward, CA 94542, USA
[p]Deutsches Elektronen Synchrotron (DESY), Platanenallee 6, D-15738 Zeuthen, Germany
[q]Instituto de Astronomía, Universidad Nacional Autónoma de México, Ciudad de México, Mexico
[r]School of Physics & Center for Relativistic Astrophysics, Georgia Institute of Technology, 837 State Street NW, Atlanta, GA 30332-0430, USA
[s]Santa Cruz Institute for Particle Physics and Department of Physics, University of California, Santa Cruz, CA 95064, USA
[t]Fred Lawrence Whipple Observatory, Harvard-Smithsonian Center for Astrophysics, Amado, AZ 85645, USA
[u]CTAO, Saupfercheckweg 1, 69117 Heidelberg, Germany
[v]Department of Physics and Astronomy, University of Alabama, Tuscaloosa, AL 35487, USA

Ground-based and Airborne Telescopes VIII, edited by Heather K. Marshall, Jason Spyromilio, Tomonori Usuda, Proc. of SPIE Vol. 11445, 114456A · © 2020 SPIE
CCC code: 0277-786X/20/$21 · doi: 10.1117/12.2564653

[w]Department of Physics and Astronomy, University of Iowa, Iowa City, IA 52242, USA
[x]Department of Physics and Astronomy, University of Utah, Salt Lake City, UT 84112, USA
[y]Department of Physics and Astronomy, University of California, Los Angeles, CA 90095, USA
[z]Department of Physics and Astronomy, University of Pennsylvania, Philadelphia, PA 19104, USA
[aa]Department of Physics and Wisconsin IceCube Particle Astrophysics Center, University of Wisconsin, Madison, WI 53706, USA
[ab]Instituto de Física de Partículas y del Cosmos, Universidad Complutense de Madrid, Spain
[ac]Institute for Space–Earth Environmental Research and Kobayashi–Maskawa Institute for the Origin of Particles and the Universe, Nagoya University, Nagoya 464-8601, Japan
[ad]INAF - IASF Milano, Italy
[ae]Dipartimento di Scienze Fisiche, della Terra e dell'Ambiente, Università degli Studi di Siena, Siena, Italy
[af]INAF - Osservatorio Astronomico di Brera, Milano/Merate, Italy
[ag]Citadel Securities LLC, Chicago, IL 60603, USA
[ah]Subaru Telescope NAOJ, Hilo HI 96720, USA
[ai]INFN Sezione di Pisa, Pisa, Italy
[aj]ASI Italian Space Agency, Roma, 00133, Italy
[ak]CNR-ISASI, Italy
[al]Enrico Fermi Institute, University of Chicago, Chicago, IL 60637, USA
[am]School of Physics and Astronomy, University of Minnesota, Minneapolis, MN 55455, USA

ABSTRACT

The novel 9.7m Schwarzschild-Couder Telescope (SCT), utilizing aspheric dual-mirror optical system, has been constructed as a prototype medium size γ-ray telescope for the Cherenkov Telescope Array (CTA) observatory. The prototype SCT (pSCT) is designed to achieve simultaneously the wide ($\geq 8^\circ$) field of view and the superior imaging resolution (0.067° per pixel) to significantly improve scientific capabilities of the observatory in conducting the sky surveys, the follow-up observations of multi-messenger transients with poorly known initial localization and the morphology studies of γ-ray sources with angular extent. In this submission, we describe the hardware and software implementations of the telescope optical system as well as the methods specifically developed to align its complex optical system, in which both primary and secondary mirrors are segmented. The pSCT has detected Crab Nebula in June 2020 during ongoing commissioning, which was delayed due to worldwide pandemic and is not yet completed. Verification of pSCT performance is continuing and further improvement of optical alignment is anticipated.

Keywords: Imaging Cherenkov Telescopes, Aplanatic Optical System, Gamma Ray

1. INTRODUCTION

The success of the ground-based γ-ray detection technology offered by the small arrays of imaging atmospheric Cherenkov telescopes (IACTs) has firmly established the field of astronomy and astrophysics at photon energies above 100 GeV. The very high-energy (VHE) γ-rays produced by the most violent events in the cosmos create particle cascades when interacting with the Earth atmosphere. Numerous secondary particles of these cascades emit Cherenkov light in the wavelength band between 250 and 800 nm. The IACTs are designed to collect as many Cherenkov photons as possible during a short exposure of the Cherenkov light pulse, which duration is roughly 6 to 200 ns depending on the observing conditions and the energy of the primary particle. The images of the atmospheric cascades are recorded by IACT arras and are used to reconstruct arrival direction of the

[†] E-mails: , vvv@astro.ucla.edu

primary photon and its energy and, hence, the imaging resolution of IACT camera is an important performance characteristic as it directly affects the γ-ray angular resolution and the discrimination power against the cosmic-ray-induced background that dominates IACT triggers.

The present-day IACTs are based on conventional Davies-Cotton (DC) design of a single parabolic reflector 1. The Davies-Cotton design has been proven to be suitable and robust for detecting atmospherical Cherenkov light emissions, however, due to spherical and comatic aberrations the DC design is constrained to the photosensor technology of photo-multiplier tubes (PMTs) with limited imaging resolution. These limitations of DC design constrains the potential of the next-generation world-wide observatory Cherenkov Telescope Array (CTA) 2, 3 in searching for multi-messenger transients often with poorly known initial localization, or measuring the morphologies of the spatially extended γ-ray sources that may be connected to cosmic ray PeVatrons, which require the capacity of monitoring the full sky with wide FoV and high angular resolution.

The prototype Schwarzschild-Couder telescope (pSCT) 4, 5 implements a design of aplanatic dual-mirror optics, rapid telescope re-positioning mechanics, and highly integrated camera electronics, to provide a wide FoV of 8° with high imaging resolution of 0.067°, which can make an important impact on the key science project of CTA observatory 3. A major challenge of realizing the SCT technology comes from the alignment of the two aspherical mirrors, which are segmented into 48 and 24 panels, respectively. This submission describes the alignment hardware and software implementations as well as the alignment techniques that were developed to accomplish the alignment of pSCT optical system. The pSCT was inaugurated in January 2019 (Figure 1) and has detected Crab Nebula in June 2020. The operational phase of pSCT is in early stage, and the ongoing commissioning was interrupted by the development of the COVID-19 pandemic. The result presented in this submission doesn't represent the final performance of pSCT, which is expected to be further improved.

Figure 1: The pSCT inauguration took place in January 2019 at the Fred Lawrence Whipple Observatory (FLWO) in Tucson, Arizona.

2. OVERVIEW OF THE PSCT HARDWARE IMPLEMENTATION

The design of Schwarzschild-Couder (SC) optical system (OS) of the pSCT is chosen to fully correct spherical and comatic aberrations over the 8° FoV with its dual-mirror optical system, primary (M1) and secondary (M2) mirrors, and to minimize astigmatism by curving the surface of the focal plane 4,5. The de-magnifying secondary mirror, M2, reduces the effective focal length of the OS and the plate scale by a factor of 2.86 to the value of 1.625 mm/arcmin. This reduction allows an advanced photosensor technology of higher photon detection efficiency silicon photomultipliers (SiPMs) with 6.53×6.53 mm^2 imaging pixels.

The primary and secondary mirrors of pSCT are segmented for cost reduction. The 9.7-m primary mirror is segmented into 48 panels, and the 5.4-m secondary mirror is segmented into 24 panels. Both primary and secondary panels are aspherical, the M2 panels in particular are highly curved with a few-cm sag in each panel. The 72 aspherical mirror panels were made with industrial employment of cost-effective hot and cold glass slumping replication technologies. The segmentation types of M1 and M2 can be found in 6.

Each panel is supported by a Stewart platform with six linear actuators which provide six degrees of freedom of the motion of the panels, whose relative position with respect to the neighboring panels is monitored by several mirror-panel edge sensors (MPESs). Each actuator is equipped with a stepping motor that provides a motion range of 63 mm and is capable of moving a maximum mass of 65 kg at 500 steps/s. The MPES unit is designed with a low-power laser diode aiming at a 0.3-megapixel webcam mounted on the opposite sides of an edge between two neighboring panels. The arrangement of the MPES units on an edge is made to reduce degeneracy of the MPES readings to the panel motion 7 and is shown in Figure 2. By measuring the changes in the position of the laser spot in the webcam field of view, the MPES units is capable of monitoring the panel motion with a resolution better than 5 μm. The Stewart platform also hosts a microcomputer which is responsible for collecting data from the actuators and the MPESs as well as issuing commands to these devices. The panel, the Stewart platform, and the MPESs form a mirror panel module (MPM), and the pSCT OS is composed of 72 MPMs.

In addition to the panel-to-panel alignment system (P2PAS) based on the MPES readings, which monitors the alignment between a pair of adjacent mirror panels, a global alignment system (GAS) is responsible for the alignment between M1, M2 and the camera focal plane (FP). The GAS is composed of two optical tables (OTs) at the centers of the primary (OT1) and secondary (OT2) mirrors and a optical camera alignment module (OCAM) at the center of the camera. A reference laser beam that can be produced by a laser installed on OT1 is used to define the optical axis for the global alignment. The laser beam can be measured by the transparent position sensitive devices (PSDs) located in OCAM and OT2. The OTs are hosted by Stewart platforms so that their motions can be controlled to align the γ-ray camera with four degrees of freedom with respect to the reference laser beam. The relative translation and tip/tilt of M1 and M2 with respect to the optical axis can be monitored by GAS. The translation is measured by analyzing the images of multiple reference LEDs mounted on the selected panels of M1 and M2 taken by the three CCD camera on the OT of the opposite mirror. The tip/tilt of the mirrors with respect to the OTs is measured by two autocollimators on each OT and two retro-reflectors on a reference panel of each mirror. Lastly, OT2 is equipped with a range meter to measure the distance between OT1, FP, and M2, as well as a sky camera with the orientation fixed with respect to the optical axis, which can take continuous images of the sky for offline pointing corrections. The components of GAS are illustrated in Figure 3.

3. OVERVIEW OF THE PSCT SOFTWARE IMPLEMENTATION

To facilitate control of the many parallel devices described in the previous section, the software architecture was designed to fulfill several criteria: real-time parallel processing and monitoring of all devices, centralized control server for collecting and processing data, modular controller objects for fine-tuned access, and secure network protocol for open platform communication. These criteria are naturally met with Open Platform Communications standard with unified architecture (OPC-UA) developed by the OPC foundation as an industry standard.

The OPC-UA standard provides the framework to create controller objects for each hardware device or pseudo-hardware device described in this alignment system. In brief, controller objects act like wrappers for interacting with each device, where methods for device-specific calls can be defined and data collected using a

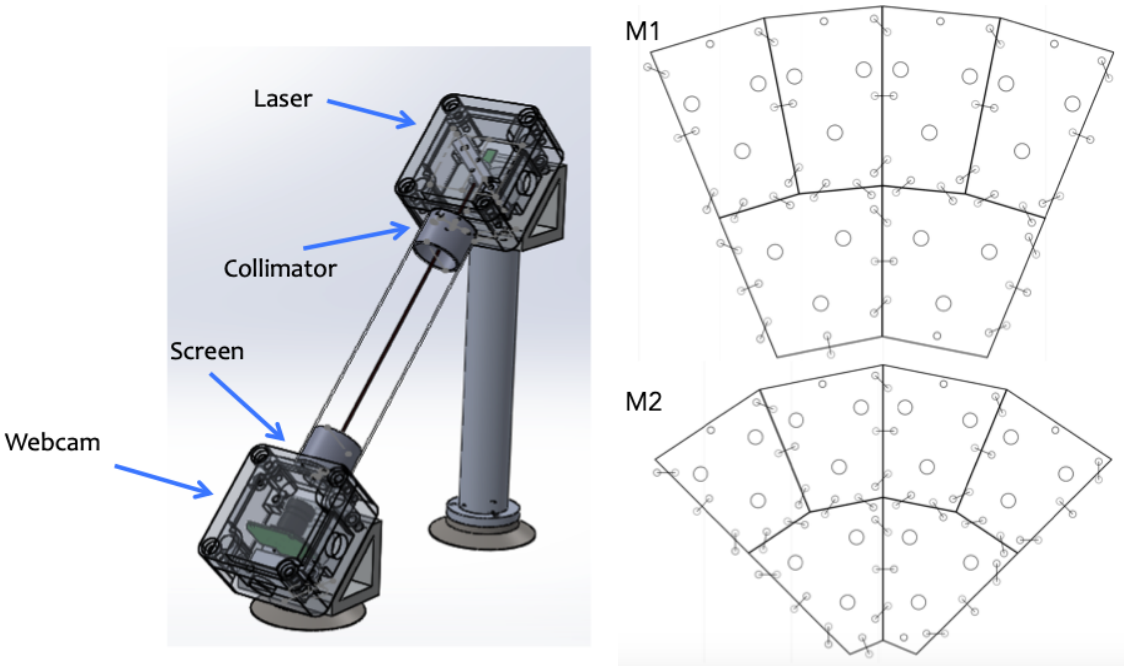

Figure 2: (Left) Each MPES unit is composed of a low-power laser diode and a 0.3-megapixel low-cost webcam located on the opposite sides of an edge between a pair of adjacent mirror panels, and the webcam measures the X and Y positions of the beam on the webcam. (Right) The orientation of the MPESs on M1 and M2. The big circles indicate the location of actuator joints, the small circles indicate the location of MPES lasers and webcams, and the short lines indicate the laser beam orientations. The laser beams of three MPES units on each "long" edge between mirror panels are arranged mutually orthogonal to completely constraining the relative six degrees of freedom of one panel with respect to its neighbor.

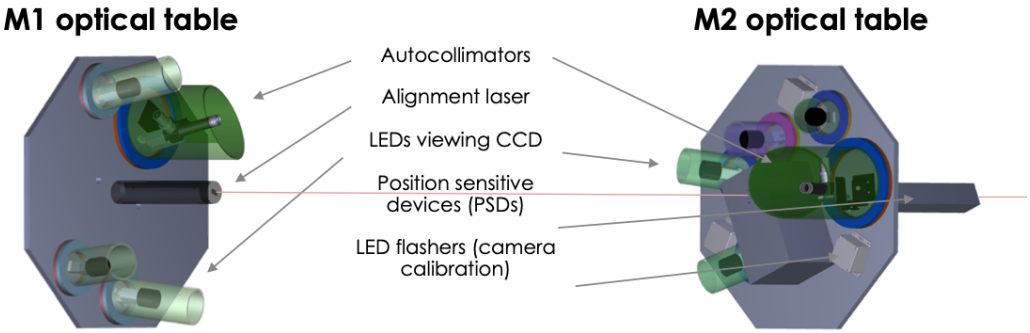

Figure 3: Illustration of the global alignment system of the pSCT. Two optical tables that host GAS devices including autocollimators (ACs), an alignment laser, position sensitive devices (PSDs), and CCD cameras, are supported by two Stewart platforms located at the centers of the two mirrors.

shared framework. Through this shared framework the controllers can interact with each other, for an arbitrary number of controllers of varying levels of abstraction, within the same persistent program.

Most importantly, this protocol functions with a server-client communication paradigm such that servers interact with controllers directly, while clients poll from and query to the server. We can map the features of the framework to our alignment software design as follows. The microcomputer within the MPM runs the server program with controllers for each actuator or MPES device connected to it, while a node management program handles communication priorities and automated tasks. For instance, MPES cannot be queried while actuators are moving due to power and bandwidth limitations, so the node manager organizes competing calls to this server with busy states and locks to ensure proper functioning. All MPMs are installed with the same server

program.

The second component to the server-client communication is the unique client running in a central alignment computer. Conventionally, server-client systems consist of a single server and an arbitrary number of clients simultaneously interacting with it. To handle the many MPM, OTs and other servers in our system, we developed a server-client hybrid that ultimately functions as our central "client", hereafter simply named client. This hybrid designation evolves from the creation of an aggregation server that communicates with all MPMs and OTs like a client, while simultaneously acting like a server for a higher level client to interact with. Due to communication limits, we developed four intermediate aggregation servers, each limited to 24 MPM or OTs, and one top level client accessible to the user.

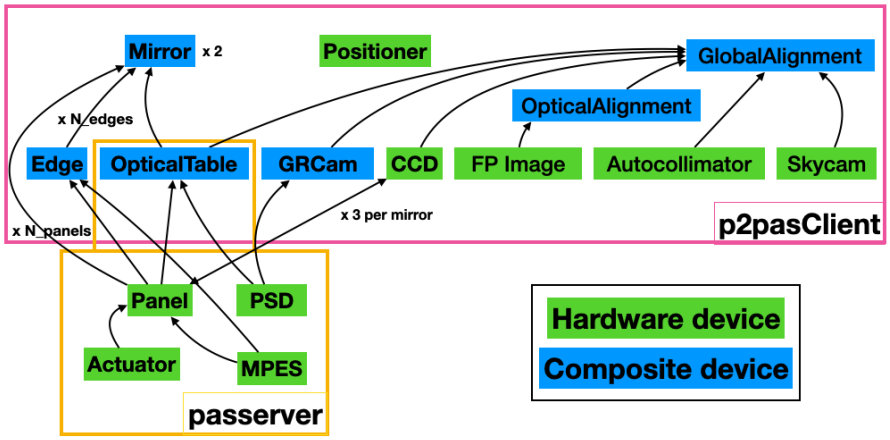

Figure 4: Device tree showing relationship between all the controllers within the alignment software. Controllers are object instances within the p2pasClient (pink) or passerver (orange) binaries. Hardware devices in green map directly to hardware controllers, while composite devices in blue are collections of hardware devices as a pseudo-hardware object.

Fig. 4 shows the hierarchy of controllers within the client and server systems. Notably, some controllers map directly to physical hardware devices such as MPES, actuators or CCDs, while others are pseudo-hardware objects called composite devices. These composite devices are collections of multiple hardware devices, such as panels (MPES and actuators together), edges (multiple panels) or mirrors (full collection of multiple panels to complete a mirror). Separating hardware and composite devices helps to demarcate the true hardware objects that must be physically maintained and serviced in the field from those that need software intervention.

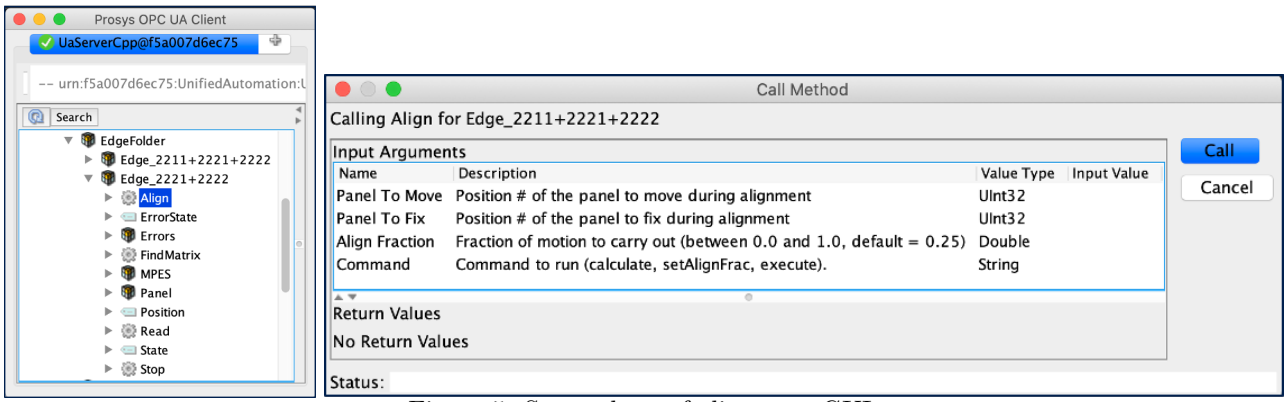

Figure 5: Screenshots of alignment GUI.

Two features of this software design are important to highlight in this section due to their significance in complex alignment tasks described in later sections: 1) parallelization achieved by the use of OPC-UA asynchronous

method, and 2) effective controller abstraction to enable non-conventional techniques such as the freezing of a single degree of freedom across full mirror alignment. Parallelization was primarily enabled by asynchronous calls to the server from the client relying on the asynchronous method management provided by the OPC-UA node manager class. These calls are sanitized by a simple, custom thread-locking class that ensures mutually exclusive controllers have completed their actions before starting new actions remaining in the queue. A few examples of parallelization include simultaneous reading of all MPES, synchronized actuator stepping to smoothly move panels and synchronized panel motion for effective whole-mirror translations and rotations in the telescope reference frame.

In the second feature, we learned from experience how to reduce controller abstraction so that it would be possible to construct complex alignment methods with arbitrary constraints. The mirror composite device was created, deploying methods that inherited directly from the underlying panel class able to move in the panel reference frame rather than actuator lengths. This improved controller abstraction enables the writing of methods that can include the freezing of whole mirror degrees of freedom such as the T_z dimension or R_x and R_y rotations. It was then straightforward to maintain dipole/quadrupole pertubation corrections while rotating in R_x and R_y by keeping T_z fixed.

4. MPES GUIDED ALIGNMENT METHODS

Before the installation of the MPMs on the telescope, the MPES units were calibrated in the laboratory in order to provide the reference MPES readings for the MPES guided alignment. Each MPM was assembled with six actuators that connect a mounting triangle and a mirror panel. Every pair of neighboring MPMs were mounted on a laboratory optical table and aligned with a coordinate measuring machine (CMM), which uses a mechanical Renishaw touch probe to measure the locations of the predefined spots on the mirror surfaces. After the edge was aligned, the MPES units along the edge were installed, the readings of the MPES units were recorded as the initial aligned state, and the corresponding actuator-MPES response matrices were also measured and recorded in the database. The calibrated panels were then installed onto the telescope optical system structure on site for commissioning. During the installation of the panels, every MPES was made sure that its laser spot fell within its camera's field of view of 12 mm diameter and served as a base alignment position prior to edge optimization.

The six degrees of freedom of a mirror panel (translation in T_x, T_y, T_z, and rotations in R_x, R_y, R_z), with respect to the x, y, z axes in the panel reference frame, are controlled by the six supporting actuators. The relative motion of a panel with respect to its neighbors are monitored by the MPES units. The mapping of the MPES readings to the actuator motions is described by a response matrix. On a single edge $M\vec{\delta} = \vec{\Delta}$, where $\vec{\delta} = [\delta_1, \cdots, \delta_6]$ is the vector of actuator motion, $\vec{\Delta} = [\Delta_{x1}, \Delta_{y1}, \cdots, \Delta_{x3}, \Delta_{y3}]$ is the corresponding vector of change in the MPES readings in the frame of camera field of view, and M is the response matrix. The alignment of a single edge is achieved by solving the required panel motion to minimize the MPES reading displacements, i.e. $\vec{\delta} = M^{-1}\vec{\Delta}$. The single-edge alignment can be extended to a mirror-wide alignment, where all MPES units and actuators are included into the vector $\vec{\Delta}$ and $\vec{\delta}$.

The MPES guided alignment has no constraint on the global motion of the mirror and very little constraint on the large-spatial-scale mis-alignments. The large-spatial-scale mis-alignments, such as dipole and quadruple perturbation modes, can be induced by the systematic errors of the lab calibrations and accumulate only small distortions at each edge. These small distortions are difficult to correct with the MPES guided alignment, and special alignment methods are developed to address these problems.

Due to its large surface curvature, the lab calibration of M2 panels has more significant systematic errors comparing to the calibration of M1 panels. These systematic errors lead to a dipole-like distortion in the panel T_z positions as well as distortions in other degrees of freedom. The distribution of the panel T_z positions was Fourier decomposed, and the panels were moved manually in T_z to compensate the observed dipole and quadruple modes. Once the dipole and quadruple perturbations in panel T_z positions are removed, a few panels are selected and fixed to maintain the global motion of the whole mirror, and the rest of panels are aligned to these reference panels with their T_z position fixed during alignment.

The PSF and image variations on the focal plane are sensitive to the rotational degrees of freedom of the panels, R_x and R_y. The defocused star images, which will be further discussed in Section 5, are used to aid the

MPES guided alignment. The mis-aligned R_x and R_y panel positions produce randomly scattered spots of the reflection of a bright star. These spots, which were reflected from certain panels, were identified and rearranged into a pattern structure. The arrangement of the spots into the pattern effectively align the R_x and R_y positions of the panels. Once the R_x and R_y positions are determined, the rest of the degrees of freedom (T_x, T_y, T_z, R_z) of the panels are aligned using MPES with the R_x and R_y of each panel fixed.

The MPES-guided alignment procedure can only be realized thanks to the development of software that is capable of parallel processing of multiple panels and/or sensors, as it is discussed in Section 3. The capacity of processing multiple elements not only allow aligning multiple panels simultaneously, but also enable the creation of a "pseudo" solid body of a collection of panels that could move in the telescope reference frame. The special regularization methods for alignments, such as fixing certain degrees of freedom and/or freezing selected panels, are also crucial to the large-scale panel-to-panel alignments.

The MPES-guided alignment procedure has brought the panel-to-panel alignment to a MPES offset average of ≈ 300 μm with respect to the lab-calibrated reference MPES readings. The distribution of measured MPES offsets after the MPES alignment procedure can be found in 6. It should be noted that the current MPES-guided alignment, which is expected to provide an accuracy of alignment on the order of ≈ 50 μm or better, does not achieve its full capacity due to the challenge of the systematic errors introduced in the lab calibrations. After the precise optical alignment, which is discussed in the Section 5, the reference MPES readings will be updated in the database replacing laboratory measurements.

5. STRATEGIES FOR ALIGNMENT USING DEFOCUSED IMAGES OF STARS

The optical PSF is most sensitive to the tip/tilt rotation of the M1 panels and the translation of M2 panels. Therefore, further alignment strategies designed to constrain these degrees of freedom is needed in addition to the MPES-guided alignment. In this section, we describe one of such alignment methods, *alignment using defocused images of stars*, employed in the commissioning alignment process.

To describe the *alignment using defocused images of stars*, it is necessary to first establish the number of optical images from a misaligned/defocused OS. The 16 primary inner (P1) panels reflect on-axis light onto the secondary inner (S1) panels, and produce 16 images. The 32 primary outer (P2) panels reflect on-axis light onto both secondary outer (S2) and S1 panels, and produce 64 images. Therefore, there is a total of 80 images of one on-axis star. Note that these images would overlap at the focal point if the OS is aligned, while a maximum of 80 non-overlapping images can result from one on-axis star if all panels are misaligned.

The goal of *alignment using defocused images of stars* is to focus the pSCT OS, i.e., to find the configurations of each panel so that all 80 optical images from pairs of M1-M2 panels overlap at the focal point (correct distances between M1, M2, and camera are implied).

This method uses the displacement between an optical image of an on-axis star with respect to the focal point to guide the precise tip/tilt rotation of a M1 panel in order to achieve alignment. It also uses the spread area and elongation of these optical images to guide the adjustment of the relative placement of M2 with respect to the gamma-ray camera. As a result, the *alignment using defocused images of stars* directly optimizes the optical PSF and offers strong constraints on the tip-tilt of the M1 optical surfaces, as well as the global translation and tip-tilt of the entire M2 mirror.

A description of the detailed alignment procedure using defocused images of stars can be found in 6.

A response matrix that maps a translation of the centroid of an image of a star to a tip-tilt rotation of a corresponding panel is necessary for this alignment process. With the response matrices, it is possible to calculate the amount of relative rotation of a panel that moves the image of the star reflected from the same panel by any given amount (e.g., form an arbitrary position to the focal point for alignment). These response matrices were initially measured with one panel rotating at a time, which also allowed image/panel association.

After all images are associated with pairs of panels and initial response matrices are measured, the optical images can be organized in a circular pattern that resembles the layout of the panels. This is to facilitate easy identification of images and efficient alignment using defocused images of stars. This is termed as a "defocused"

pattern, allowing rapid parallel measurements of all response matrices and therefore rapid re-alignment of the OS as needed when OSS deformation occurs as external conditions (e.g., temperature) or telescope pointing change.

The optical images of a bright on-axis star on the focal plane taken with two defocused configurations and the initially focused configuration of the pSCT OS are shown in Figure 6. The *left* panel shows a three-ring defocused configuration, in which S1 and S2 panels are intentionally misaligned to separate images from P2 panels. By aligning S2 panels with respect to S1 panels, the images in the outer ring shown in the *left* panel move inward and merge with the middle ring, leaving only two rings, as shown in the *center* panel. Then P1 and P2 panels can be rotated so that the all images move to the center of the focal plane, as shown in the *right* panel. At this configuration, the tip/tilt rotation of M1 panels are considered aligned.

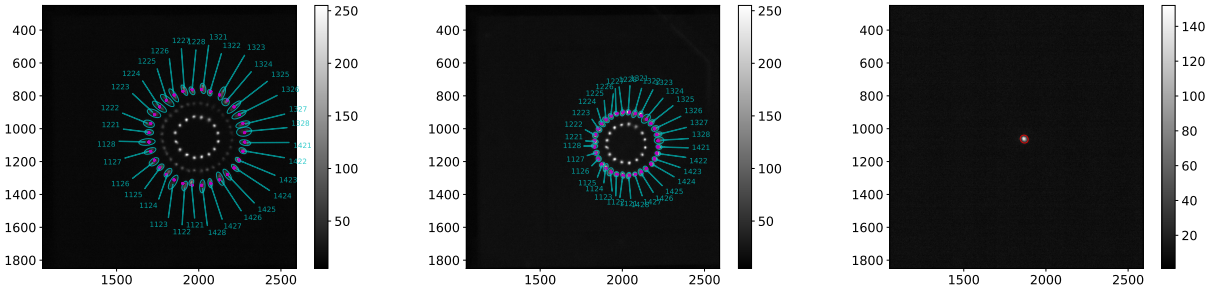

Figure 6: Illustrations of the optical alignment using defocused images of an on-axis star. (*left*) Defocused optical images of a bright on-axis star with P2 panels identified at the images produced by P2-S2 pairs. (*center*) Defocused images of the same on-axis star with S1-S2 panels aligned so that the images in the outer circle (P2-S2 images) in the *left* panel merged with the images in the middle circle (P2-S1 images). (*right*) Optical images of a bright on-axis star with the OS in focus. All images shown cover about a 3.5° field with the focal point and the pSCT camera roughly in the center.

Besides the tip/tilt rotation of M1 panels, the *alignment using defocused images of stars* can also guide the relative placement of M2 with respect to the focal plane, which is also critical to the optical PSF. The initial focus of the SC OS was achieved by adjusting the distance between the focal plane and M2 mirror to minimize the area of the optical images of defocused stars. It is then possible to adjust the global tip-tilt rotation of the M2 mirror from the "defocused" configuration so that any dipole moment of the ellipticity/elongation of all the images is removed. The minimization of the image area and the removal of dipole moment of the ellipticity allow a desired relative placement, in both translation and rotation, of the M2 mirror with respect to the focal plane that optimizes the optical PSF.

The off-axis optical PSF of pSCT, a crucial performance measure that ensures the unique advantages of the SCT OS design, is yet to be studied. A set of images with an off-axis star at various offsets were taken to search for any substantial degradation of the optical images from individual pairs of panels. The contours extracted with the `astrometry.net` tool from these images are shown in Figure 7. These images were taken in October, 2019, before the commissioning alignment was reached. No substantial degradation of the image were found in this initial verification. Note that the exposures of these images were not necessarily uniform, and the ambient light condition may have changed, making a few images difficult to parameterize, as illustrated by the few large ellipses.

6. ON-AXIS PSF PERFORMANCE

An on-axis optical PSF of 2.8 arcmin (shown in Figure 8) 6 has been achieved during the phase of initial commissioning of the pSCT in December 2019, after employing first the MPES-based alignment and then a few iterations of alignment using defocused images of stars.

The commissioning on-axis optical PSF of 2.8 arcmin is superior than the "acceptable" on-axis PSF of 3.6 arcmin, and only 8% worse than the "goal" of 2.6 arcmin, both of which were defined in the report during the pSCT pre-construction readiness review conducted by the CTA project in 2013.

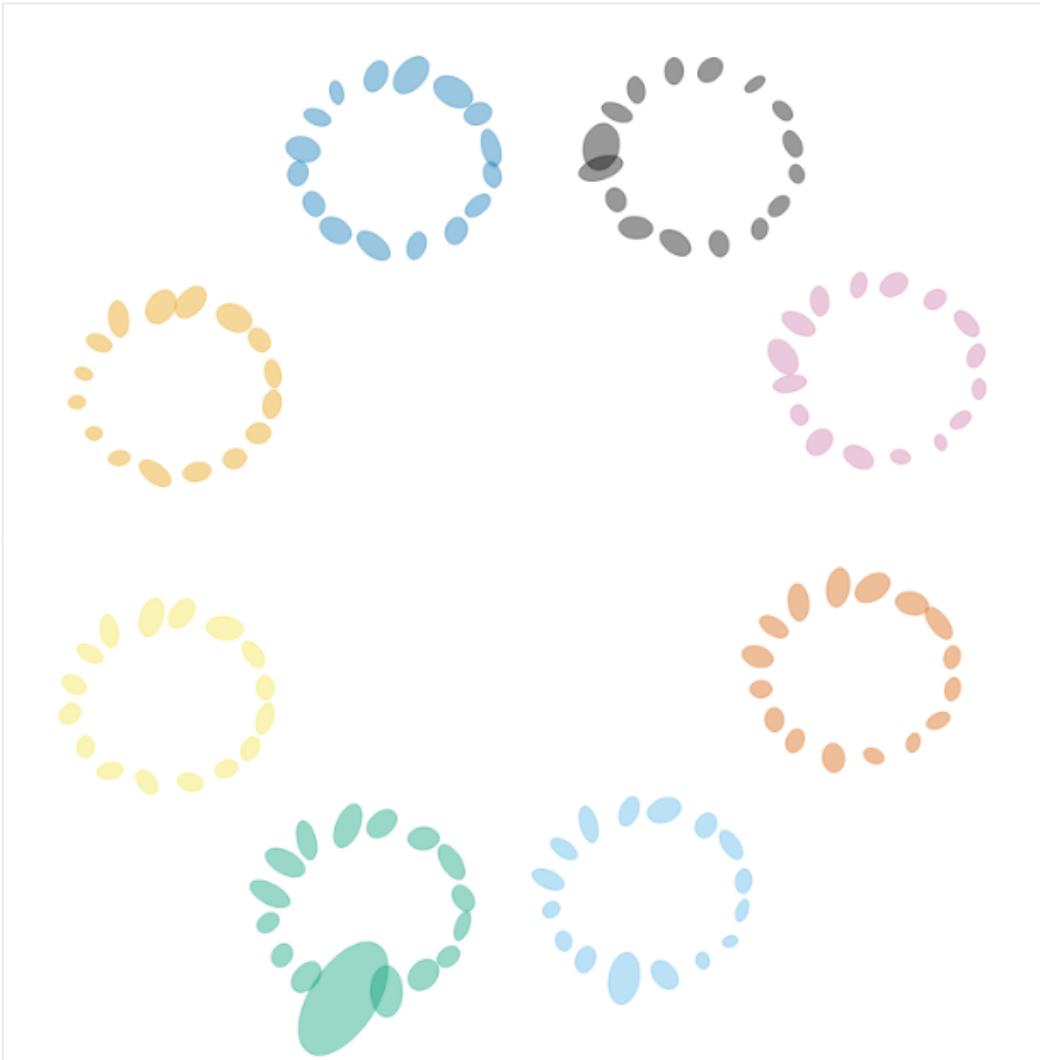

Figure 7: Illustrations of the images of an off-axis star at eight different offsets from the center of the FoV. The contours identified with the `astrometry.net` tool for the P1-S1 images (inner ring) are shown. No obvious degradation of the PSF is apparent.

The sizes of a 4-arcmin pSCT "imaging" pixel and an 8-arcmin pSCT "trigger" pixel (consists of four "imaging" pixels) are illustrated by the white unfilled squares in Figure 8. The commissioning optical alignment achieved a 75.5% containtment of the PSF within the size of an "imaging" SiPM pixel, and a 99.5% containment within a "trigger" pixel (defined as 2×2 imaging pixels) for the pSCT. These results serve as a first verification 6 of the on-axis performance of the SCT OS in a telescope with a 9.7-m aperture with both primary and secondary mirrors segmented. Therefore, the SCT is considered a viable contender for the medium-sized telescope of CTA from the perspectives of technology and cost. The advantages of the Schwarzschild-Couder OS for science in ground-based γ-ray astronomy will in turn benefit the CTA experiment.

ACKNOWLEDGMENTS

We gratefully acknowledge support from the agencies and organizations listed under Funding Agencies at this website: www.cta-observatory.org. The development of the prototype SCT has been made possible by funding provided through the NSF-MRI program under awards PHY-1229792, PHY-1229205, and PHY-1229654. The authors are also grateful for the generous support of the National Science Foundation under awards PHY-1607491,

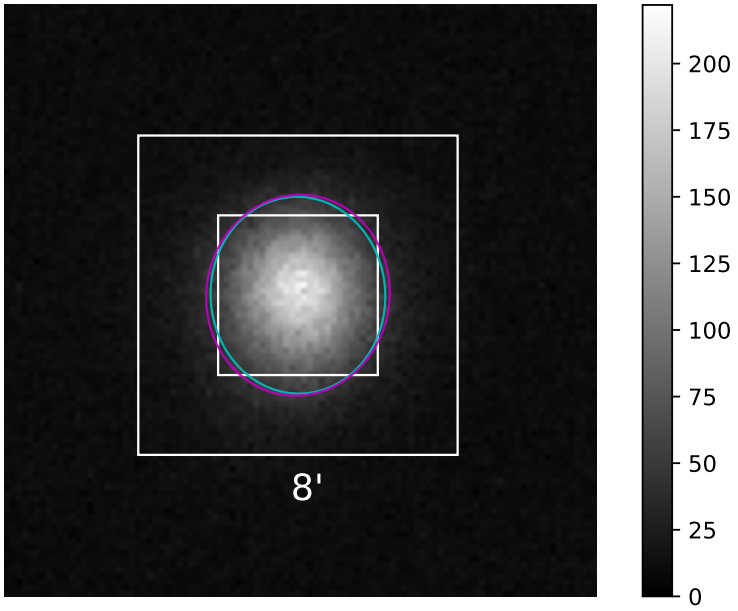

Figure 8: The optical PSF of the pSCT illustrated by an image of an on-axis star (Capella) on the focal plane, taken during the initial commissioning campaign in December 2019. The cyan ellipse shows the 1.8-σ ($\sim$80% containment) contour from the best 2D Gaussian fit. The magenta contour shows the extension solution obtained from the `astrometry.net` tool. The two contours are roughly in agreement. The inner and outer white unfilled squares illustrate the sizes of a 4-arcmin pSCT "imaging" pixel and an 8-arcmin pSCT "trigger" pixel (consists of four "imaging" pixels), respectively.

PHY-1352567, PHY-1505811, PHY-1806554, and PHY-1913798. We are grateful to INAF for having supported part of the M2 production.

REFERENCES

[1] Davies, J. M. and Cotton, E. S., "Design of the quartermaster solar furnace," *Solar Energy* **1**, 16–22 (Apr 1957).

[2] Actis, M., Agnetta, G., Aharonian, F., Akhperjanian, A., Aleksić, J., Aliu, E., Allan, D., Allekotte, I., Antico, F., Antonelli, L. A., Antoranz, P., Aravantinos, A., Arlen, T., Arnaldi, H., Artmann, S., Asano, K., Asorey, H., Bähr, J., Bais, A., Baixeras, C., Bajtlik, S., Balis, D., Bamba, A., Barbier, C., Barceló, M., Barnacka, A., Barnstedt, J., Barres de Almeida, U., Barrio, J. A., Basso, S., Bastieri, D., Bauer, C., Becerra, J., Becherini, Y., Bechtol, K., Becker, J., Beckmann, V., Bednarek, W., Behera, B., Beilicke, M., Belluso, M., Benallou, M., Benbow, W., Berdugo, J., Berger, K., Bernardino, T., Bernlöhr, K., Biland, A., Billotta, S., Bird, T., Birsin, E., Bissaldi, E., Blake, S., Blanch, O., Bobkov, A. A., Bogacz, L., Bogdan, M., Boisson, C., Boix, J., Bolmont, J., Bonanno, G., Bonardi, A., Bonev, T., Borkowski, J., Botner, O., Bottani, A., Bourgeat, M., Boutonnet, C., Bouvier, A., Brau-Nogué, S., Braun, I., Bretz, T., Briggs, M. S., Brun, P., Brunetti, L., Buckley, J. H., Bugaev, V., Bühler, R., Bulik, T., Busetto, G., Buson, S., Byrum, K., Cailles, M., Cameron, R., Canestrari, R., Cantu, S., Carmona, E., Carosi, A., Carr, J., Carton, P. H., Casiraghi, M., Castarede, H., Catalano, O., Cavazzani, S., Cazaux, S., Cerruti, B., Cerruti, M., Chadwick, P. M., Chiang, J., Chikawa, M., Cieślar, M., Ciesielska, M., Cillis, A., Clerc, C., Colin, P., Colomé, J., Compin, M., Conconi, P., Connaughton, V., Conrad, J., Contreras, J. L., Coppi, P., Corlier, M., Corona, P., Corpace, O., Corti, D., Cortina, J., Costantini, H., Cotter, G., Courty, B., Couturier, S., Covino, S., Croston, J., Cusumano, G., Daniel, M. K., Dazzi, F., de Angelis, A., de Cea Del Pozo, E., de Gouveia Dal Pino, E. M., de Jager, O., de La Calle Pérez, I., de La Vega, G., de Lotto, B., de Naurois, M., de Oña Wilhelmi, E., de Souza, V., Decerprit, B., Deil, C., Delagnes, E., Deleglise, G., Delgado, C., Dettlaff, T., di Paolo, A., di Pierro, F., Díaz, C.,

Dick, J., Dickinson, H., Digel, S. W., Dimitrov, D., Disset, G., Djannati-Ataï, A., Doert, M., Domainko, W., Dorner, D., Doro, M., Dournaux, J. L., Dravins, D., Drury, L., Dubois, F., Dubois, R., Dubus, G., Dufour, C., Durand, D., Dyks, J., Dyrda, M., Edy, E., Egberts, K., Eleftheriadis, C., Elles, S., Emmanoulopoulos, D., Enomoto, R., Ernenwein, J. P., Errando, M., Etchegoyen, A., Falcone, A. D., Farakos, K., Farnier, C., Federici, S., Feinstein, F., Ferenc, D., Fillin-Martino, E., Fink, D., Finley, C., Finley, J. P., Firpo, R., Florin, D., Föhr, C., Fokitis, E., Font, L., Fontaine, G., Fontana, A., Förster, A., Fortson, L., Fouque, N., Fransson, C., Fraser, G. W., Fresnillo, L., Fruck, C., Fujita, Y., Fukazawa, Y., Funk, S., Gäbele, W., Gabici, S., Gadola, A., Galante, N., Gallant, Y., García, B., García López, R. J., Garrido, D., Garrido, L., Gascón, D., Gasq, C., Gaug, M., Gaweda, J., Geffroy, N., Ghag, C., Ghedina, A., Ghigo, M., Gianakaki, E., Giarrusso, S., Giavitto, G., Giebels, B., Giro, E., Giubilato, P., Glanzman, T., Glicenstein, J. F., Gochna, M., Golev, V., Gómez Berisso, M., González, A., González, F., Grañena, F., Graciani, R., Granot, J., Gredig, R., Green, A., Greenshaw, T., Grimm, O., Grube, J., Grudzińska, M., Grygorczuk, J., Guarino, V., Guglielmi, L., Guilloux, F., Gunji, S., Gyuk, G., Hadasch, D., Haefner, D., Hagiwara, R., Hahn, J., Hallgren, A., Hara, S., Hardcastle, M. J., Hassan, T., Haubold, T., Hauser, M., Hayashida, M., Heller, R., Henri, G., Hermann, G., Herrero, A., Hinton, J. A., Hoffmann, D., Hofmann, W., Hofverberg, P., Horns, D., Hrupec, D., Huan, H., Huber, B., Huet, J. M., Hughes, G., Hultquist, K., Humensky, T. B., Huppert, J. F., Ibarra, A., Illa, J. M., Ingjald, J., Inoue, Y., Inoue, S., Ioka, K., Jablonski, C., Jacholkowska, A., Janiak, M., Jean, P., Jensen, H., Jogler, T., Jung, I., Kaaret, P., Kabuki, S., Kakuwa, J., Kalkuhl, C., Kankanyan, R., Kapala, M., Karastergiou, A., Karczewski, M., Karkar, S., Karlsson, N., Kasperek, J., Katagiri, H., Katarzyński, K., Kawanaka, N., Kędziora, B., Kendziorra, E., Khélifi, B., Kieda, D., Kifune, T., Kihm, T., Klepser, S., Kluźniak, W., Knapp, J., Knappy, A. R., Kneiske, T., Knödlseder, J., Köck, F., Kodani, K., Kohri, K., Kokkotas, K., Komin, N., Konopelko, A., Kosack, K., Kossakowski, R., Kostka, P., Kotuła, J., Kowal, G., Kozioł, J., Krähenbühl, T., Krause, J., Krawczynski, H., Krennrich, F., Kretzschmann, A., Kubo, H., Kudryavtsev, V. A., Kushida, J., La Barbera, N., La Parola, V., La Rosa, G., López, A., Lamanna, G., Laporte, P., Lavalley, C., Le Flour, T., Le Padellec, A., Lenain, J. P., Lessio, L., Lieunard, B., Lindfors, E., Liolios, A., Lohse, T., Lombardi, S., Lopatin, A., Lorenz, E., Lubiński, P., Luz, O., Lyard, E., Maccarone, M. C., Maccarone, T., Maier, G., Majumdar, P., Maltezos, S., Małkiewicz, P., Mañá, C., Manalaysay, A., Maneva, G., Mangano, A., Manigot, P., Marín, J., Mariotti, M., Markoff, S., Martínez, G., Martínez, M., Mastichiadis, A., Matsumoto, H., Mattiazzo, S., Mazin, D., McComb, T. J. L., McCubbin, N., McHardy, I., Medina, C., Melkumyan, D., Mendes, A., Mertsch, P., Meucci, M., Michałowski, J., Micolon, P., Mineo, T., Mirabal, N., Mirabel, F., Miranda, J. M., Mirzoyan, R., Mizuno, T., Moal, B., Moderski, R., Molinari, E., Monteiro, I., Moralejo, A., Morello, C., Mori, K., Motta, G., Mottez, F., Moulin, E., Mukherjee, R., Munar, P., Muraishi, H., Murase, K., Murphy, A. S., Nagataki, S., Naito, T., Nakamori, T., Nakayama, K., Naumann, C., Naumann, D., Nayman, P., Nedbal, D., Niedźwiecki, A., Niemiec, J., Nikolaidis, A., Nishijima, K., Nolan, S. J., Nowak, N., O'Brien, P. T., Ochoa, I., Ohira, Y., Ohishi, M., Ohka, H., Okumura, A., Olivetto, C., Ong, R. A., Orito, R., Orr, M., Osborne, J. P., Ostrowski, M., Otero, L., Otte, A. N., Ovcharov, E., Oya, I., Oziębło, A., Paiano, S., Pallota, J., Panazol, J. L., Paneque, D., Panter, M., Paoletti, R., Papyan, G., Paredes, J. M., Pareschi, G., Parsons, R. D., Paz Arribas, M., Pedaletti, G., Pepato, A., Persic, M., Petrucci, P. O., Peyaud, B., Piechocki, W., Pita, S., Pivato, G., Płatos, Ł., Platzer, R., Pogosyan, L., Pohl, M., Pojmański, G., Ponz, J. D., Potter, W., Prandini, E., Preece, R., Prokoph, H., Pühlhofer, G., Punch, M., Quel, E., Quirrenbach, A., Rajda, P., Rando, R., Rataj, M., Raue, M., Reimann, C., Reimann, O., Reimer, A., Reimer, O., Renaud, M., Renner, S., Reymond, J. M., Rhode, W., Ribó, M., Ribordy, M., Rico, J., Rieger, F., Ringegni, P., Ripken, J., Ristori, P., Rivoire, S., Rob, L., Rodriguez, S., Roeser, U., Romano, P., Romero, G. E., Rosier-Lees, S., Rovero, A. C., Roy, F., Royer, S., Rudak, B., Rulten, C. B., Ruppel, J., Russo, F., Ryde, F., Sacco, B., Saggion, A., Sahakian, V., Saito, K., Saito, T., Sakaki, N., Salazar, E., Salini, A., Sánchez, F., Sánchez Conde, M. Á., Santangelo, A., Santos, E. M., Sanuy, A., Sapozhnikov, L., Sarkar, S., Scalzotto, V., Scapin, V., Scarcioffolo, M., Schanz, T., Schlenstedt, S., Schlickeiser, R., Schmidt, T., Schmoll, J., Schroedter, M., Schultz, C., Schultze, J., Schulz, A., Schwanke, U., Schwarzburg, S., Schweizer, T., Seiradakis, J., Selmane, S., Seweryn, K., Shayduk, M., Shellard, R. C., Shibata, T., Sikora, M., Silk, J., Sillanpää, A., Sitarek, J., Skole, C., Smith, N., Sobczyńska, D., Sofo Haro, M., Sol, H., Spanier, F., Spiga, D., Spyrou, S., Stamatescu, V., Stamerra, A., Starling, R. L. C., Stawarz, Ł., Steenkamp, R., Stegmann, C., Steiner, S., Stergioulas, N., Sternberger, R., Stinzing, F., Stodulski, M., Straumann, U., Suárez, A., Suchenek, M., Sugawara, R., Sulanke, K. H., Sun, S.,

Supanitsky, A. D., Sutcliffe, P., Szanecki, M., Szepieniec, T., Szostek, A., Szymkowiak, A., Tagliaferri, G., Tajima, H., Takahashi, H., Takahashi, K., Takalo, L., Takami, H., Talbot, R. G., Tam, P. H., Tanaka, M., Tanimori, T., Tavani, M., Tavernet, J. P., Tchernin, C., Tejedor, L. A., Telezhinsky, I., Temnikov, P., Tenzer, C., Terada, Y., Terrier, R., Teshima, M., Testa, V., Tibaldo, L., Tibolla, O., Tluczykont, M., Todero Peixoto, C. J., Tokanai, F., Tokarz, M., Toma, K., Torres, D. F., Tosti, G., Totani, T., Toussenel, F., Vallania, P., Vallejo, G., van der Walt, J., van Eldik, C., Vand enbroucke, J., Vankov, H., Vasileiadis, G., Vassiliev, V. V., Vegas, I., Venter, L., Vercellone, S., Veyssiere, C., Vialle, J. P., Videla, M., Vincent, P., Vink, J., Vlahakis, N., Vlahos, L., Vogler, P., Vollhardt, A., Volpe, F., von Gunten, H. P., Vorobiov, S., Wagner, S., Wagner, R. M., Wagner, B., Wakely, S. P., Walter, P., Walter, R., Warwick, R., Wawer, P., Wawrzaszek, R., Webb, N., Wegner, P., Weinstein, A., Weitzel, Q., Welsing, R., Wetteskind, H., White, R., Wierzcholska, A., Wilkinson, M. I., Williams, D. A., Winde, M., Wischnewski, R., Wiśniewski, Ł., Wolczko, A., Wood, M., Xiong, Q., Yamamoto, T., Yamaoka, K., Yamazaki, R., Yanagita, S., Yoffo, B., Yonetani, M., Yoshida, A., Yoshida, T., Yoshikoshi, T., Zabalza, V., Zagdański, A., Zajczyk, A., Zdziarski, A., Zech, A., Ziętara, K., Ziółkowski, P., Zitelli, V., and Zychowski, P., "Design concepts for the Cherenkov Telescope Array CTA: an advanced facility for ground-based high-energy gamma-ray astronomy," *Experimental Astronomy* **32**, 193–316 (Dec. 2011).

[3] Cherenkov Telescope Array Consortium, Acharya, B. S., Agudo, I., Al Samarai, I., Alfaro, R., Alfaro, J., Alispach, C., Alves Batista, R., Amans, J. P., Amato, E., Ambrosi, G., Antolini, E., Antonelli, L. A., Aramo, C., Araya, M., Armstrong, T., Arqueros, F., Arrabito, L., Asano, K., Ashley, M., Backes, M., Balazs, C., Balbo, M., Ballester, O., Ballet, J., Bamba, A., Barkov, M., Barres de Almeida, U., Barrio, J. A., Bastieri, D., Becherini, Y., Belfiore, A., Benbow, W., Berge, D., Bernardini, E., Bernardini, M. G., Bernardos, M., Bernlöhr, K., Bertucci, B., Biasuzzi, B., Bigongiari, C., Biland, A., Bissaldi, E., Biteau, J., Blanch, O., Blazek, J., Boisson, C., Bolmont, J., Bonanno, G., Bonardi, A., Bonavolontà, C., Bonnoli, G., Bosnjak, Z., Böttcher, M., Braiding, C., Bregeon, J., Brill, A., Brown, A. M., Brun, P., Brunetti, G., Buanes, T., Buckley, J., Bugaev, V., Bühler, R., Bulgarelli, A., Bulik, T., Burton, M., Burtovoi, A., Busetto, G., Canestrari, R., Capalbi, M., Capitanio, F., Caproni, A., Caraveo, P., Cárdenas, V., Carlile, C., Carosi, R., Carquín, E., Carr, J., Casanova, S., Cascone, E., Catalani, F., Catalano, O., Cauz, D., Cerruti, M., Chadwick, P., Chaty, S., Chaves, R. C. G., Chen, A., Chen, X., Chernyakova, M., Chikawa, M., Christov, A., Chudoba, J., Cieślar, M., Coco, V., Colafrancesco, S., Colin, P., Conforti, V., Connaughton, V., Conrad, J., Contreras, J. L., Cortina, J., Costa, A., Costantini, H., Cotter, G., Covino, S., Crocker, R., Cuadra, J., Cuevas, O., Cumani, P., D'Aì, A., D'Ammando, F., D'Avanzo, P., D'Urso, D., Daniel, M., Davids, I., Dawson, B., Dazzi, F., De Angelis, A., de Cássia dos Anjos, R., De Cesare, G., De Franco, A., de Gouveia Dal Pino, E. M., de la Calle, I., de los Reyes Lopez, R., De Lotto, B., De Luca, A., De Lucia, M., de Naurois, M., de Oña Wilhelmi, E., De Palma, F., De Persio, F., de Souza, V., Deil, C., Del Santo, M., Delgado, C., della Volpe, D., Di Girolamo, T., Di Pierro, F., Di Venere, L., Díaz, C., Dib, C., Diebold, S., Djannati-Ataï, A., Domínguez, A., Dominis Prester, D., Dorner, D., Doro, M., Drass, H., Dravins, D., Dubus, G., Dwarkadas, V. V., Ebr, J., Eckner, C., Egberts, K., Einecke, S., Ekoume, T. R. N., Elsässer, D., Ernenwein, J. P., Espinoza, C., Evoli, C., Fairbairn, M., Falceta-Goncalves, D., Falcone, A., Farnier, C., Fasola, G., Fedorova, E., Fegan, S., Fernand ez-Alonso, M., Fernández-Barral, A., Ferrand, G., Fesquet, M., Filipovic, M., Fioretti, V., Fontaine, G., Fornasa, M., Fortson, L., Freixas Coromina, L., Fruck, C., Fujita, Y., Fukazawa, Y., Funk, S., Füßling, M., Gabici, S., Gadola, A., Gallant, Y., Garcia, B., Garcia López, R., Garczarczyk, M., Gaskins, J., Gasparetto, T., Gaug, M., Gerard, L., Giavitto, G., Giglietto, N., Giommi, P., Giordano, F., Giro, E., Giroletti, M., Giuliani, A., Glicenstein, J. F., Gnatyk, R., Godinovic, N., Goldoni, P., Gómez-Vargas, G., González, M. M., González, J. M., Götz, D., Graham, J., Grand i, P., Granot, J., Green, A. J., Greenshaw, T., Griffiths, S., Gunji, S., Hadasch, D., Hara, S., Hardcastle, M. J., Hassan, T., Hayashi, K., Hayashida, M., Heller, M., Helo, J. C., Hermann, G., Hinton, J., Hnatyk, B., Hofmann, W., Holder, J., Horan, D., Hörandel, J., Horns, D., Horvath, P., Hovatta, T., Hrabovsky, M., Hrupec, D., Humensky, T. B., Hütten, M., Iarlori, M., Inada, T., Inome, Y., Inoue, S., Inoue, T., Inoue, Y., Iocco, F., Ioka, K., Iori, M., Ishio, K., Iwamura, Y., Jamrozy, M., Janecek, P., Jankowsky, D., Jean, P., Jung-Richardt, I., Jurysek, J., Kaaret, P., Karkar, S., Katagiri, H., Katz, U., Kawanaka, N., Kazanas, D., Khélifi, B., Kieda, D. B., Kimeswenger, S., Kimura, S., Kisaka, S., Knapp, J., Knödlseder, J., Koch, B., Kohri, K., Komin, N., Kosack, K., Kraus, M., Krause, M., Krauß, F., Kubo, H., Kukec Mezek, G., Kuroda, H., Kushida, J., La Palombara, N., Lamanna, G., Lang, R. G.,

Lapington, J., Le Blanc, O., Leach, S., Lees, J. P., Lefaucheur, J., Leigui de Oliveira, M. A., Lenain, J. P., Lico, R., Limon, M., Lindfors, E., Lohse, T., Lombardi, S., Longo, F., López, M., López-Coto, R., Lu, C. C., Lucarelli, F., Luque-Escamilla, P. L., Lyard, E., Maccarone, M. C., Maier, G., Majumdar, P., Malaguti, G., Mandat, D., Maneva, G., Manganaro, M., Mangano, S., Marcowith, A., Marín, J., Markoff, S., Martí, J., Martin, P., Martínez, M., Martínez, G., Masetti, N., Masuda, S., Maurin, G., Maxted, N., Mazin, D., Medina, C., Melandri, A., Mereghetti, S., Meyer, M., Minaya, I. A., Mirabal, N., Mirzoyan, R., Mitchell, A., Mizuno, T., Moderski, R., Mohammed, M., Mohrmann, L., Montaruli, T., Moralejo, A., Morcuende-Parrilla, D., Mori, K., Morlino, G., Morris, P., Morselli, A., Moulin, E., Mukherjee, R., Mundell, C., Murach, T., Muraishi, H., Murase, K., Nagai, A., Nagataki, S., Nagayoshi, T., Naito, T., Nakamori, T., Nakamura, Y., Niemiec, J., Nieto, D., Nikołajuk, M., Nishijima, K., Noda, K., Nosek, D., Novosyadlyj, B., Nozaki, S., O'Brien, P., Oakes, L., Ohira, Y., Ohishi, M., Ohm, S., Okazaki, N., Okumura, A., Ong, R. A., Orienti, M., Orito, R., Osborne, J. P., Ostrowski, M., Otte, N., Oya, I., Padovani, M., Paizis, A., Palatiello, M., Palatka, M., Paoletti, R., Paredes, J. M., Pareschi, G., Parsons, R. D., Pe'er, A., Pech, M., Pedaletti, G., Perri, M., Persic, M., Petrashyk, A., Petrucci, P., Petruk, O., Peyaud, B., Pfeifer, M., Piano, G., Pisarski, A., Pita, S., Pohl, M., Polo, M., Pozo, D., Prandini, E., Prast, J., Principe, G., Prokhorov, D., Prokoph, H., Prouza, M., Pühlhofer, G., Punch, M., Pürckhauer, S., Queiroz, F., Quirrenbach, A., Rainò, S., Razzaque, S., Reimer, O., Reimer, A., Reisenegger, A., Renaud, M., Rezaeian, A. H., Rhode, W., Ribeiro, D., Ribó, M., Richtler, T., Rico, J., Rieger, F., Riquelme, M., Rivoire, S., Rizi, V., Rodriguez, J., Rodriguez Fernandez, G., Rodríguez Vázquez, J. J., Rojas, G., Romano, P., Romeo, G., Rosado, J., Rovero, A. C., Rowell, G., Rudak, B., Rugliancich, A., Rulten, C., Sadeh, I., Safi-Harb, S., Saito, T., Sakaki, N., Sakurai, S., Salina, G., Sánchez-Conde, M., Sandaker, H., Sandoval, A., Sangiorgi, P., Sanguillon, M., Sano, H., Santand er, M., Sarkar, S., Satalecka, K., Saturni, F. G., Schioppa, E. J., Schlenstedt, S., Schneider, M., Schoorlemmer, H., Schovanek, P., Schulz, A., Schussler, F., Schwanke, U., Sciacca, E., Scuderi, S., Seitenzahl, I., Semikoz, D., Sergijenko, O., Servillat, M., Shalchi, A., Shellard, R. C., Sidoli, L., Siejkowski, H., Sillanpää, A., Sironi, G., Sitarek, J., Sliusar, V., Slowikowska, A., Sol, H., Stamerra, A., Stanič, S., Starling, R., Stawarz, Ł., Stefanik, S., Stephan, M., Stolarczyk, T., Stratta, G., Straumann, U., Suomijarvi, T., Supanitsky, A. D., Tagliaferri, G., Tajima, H., Tavani, M., Tavecchio, F., Tavernet, J. P., Tayabaly, K., Tejedor, L. A., Temnikov, P., Terada, Y., Terrier, R., Terzic, T., Teshima, M., Testa, V., Thoudam, S., Tian, W., Tibaldo, L., Tluczykont, M., Todero Peixoto, C. J., Tokanai, F., Tomastik, J., Tonev, D., Tornikoski, M., Torres, D. F., Torresi, E., Tosti, G., Tothill, N., Tovmassian, G., Travnicek, P., Trichard, C., Trifoglio, M., Troyano Pujadas, I., Tsujimoto, S., Umana, G., Vagelli, V., Vagnetti, F., Valentino, M., Vallania, P., Valore, L., van Eldik, C., Vand enbroucke, J., Varner, G. S., Vasileiadis, G., Vassiliev, V., Vázquez Acosta, M., Vecchi, M., Vega, A., Vercellone, S., Veres, P., Vergani, S., Verzi, V., Vettolani, G. P., Viana, A., Vigorito, C., Villanueva, J., Voelk, H., Vollhardt, A., Vorobiov, S., Vrastil, M., Vuillaume, T., Wagner, S. J., Wagner, R., Walter, R., Ward, J. E., Warren, D., Watson, J. J., Werner, F., White, M., White, R., Wierzcholska, A., Wilcox, P., Will, M., Williams, D. A., Wischnewski, R., Wood, M., Yamamoto, T., Yamazaki, R., Yanagita, S., Yang, L., Yoshida, T., Yoshiike, S., Yoshikoshi, T., Zacharias, M., Zaharijas, G., Zampieri, L., Zand anel, F., Zanin, R., Zavrtanik, M., Zavrtanik, D., Zdziarski, A. A., Zech, A., Zechlin, H., Zhdanov, V. I., Ziegler, A., and Zorn, J., [*Science with the Cherenkov Telescope Array*] (2019).

[4] Vassiliev, V., Fegan, S., and Brousseau, P., "Wide field aplanatic two-mirror telescopes for ground-based γ-ray astronomy," *Astroparticle Physics* **28**, 10–27 (Sep 2007).

[5] Vassiliev, V. and Fegan, S., "Schwarzschild-couder two-mirror telescope for ground-based gamma-ray astronomy," *arXiv preprint arXiv:0708.2741* (2007).

[6] Adams, C., Alfaro, R., Ambrosi, G., Ambrosio, M., Aramo, C., Benbow, W., Bertucci, B., Bissaldi, E., Bitossi, M., Boiano, A., Bonavolontà, C., Bose, R., Brill, A., Buckley, J. H., Byrum, K., Cameron, R. A., Capasso, M., Caprai, M., Covault, C. E., Venere, L. D., Fegan, S., Feng, Q., Fiandrini, E., Furniss, A., Garczarczyk, M., Garfias, F., Gent, A., Giglietto, N., Giordano, F., González, M. M., Halliday, R., Hervet, O., Hughes, G., Humensky, T. B., Ionica, M., Iriarte, A., Jin, W., Kaarat, P., Kieda, D., Kim, B., Licciulli, F., Limon, M., Loporchio, S., Masone, V., Meures, T., Mode, B. A. W., Mukherjee, R., Nieto, D., Okumura, A., Otte, N., Palombara, N. L., Pantaleo, F. R., Paoletti, R., Pareschi, G., Petrashyk, A., Powell, J., Powell, K., Ribeiro, D., Roache, E., Rousselle, J., Rugliancich, A., Ruíz-Díaz-Soto, J., Santander, M., Schlenstedt, S., Scuderi, S., Shang, R., Sironi, G., Stevenson, B., Stiaccini, L., Taylor, L. P., Tosti, L., Tovmassian, G.,

Vagelli, V., Valentino, M., Vandenbroucke, J., Vassiliev, V. V., Wakely, S. P., Wilcox, P., Williams, D. A., and Yu, P., "Verification of the optical system of the 9.7-m prototype Schwarzschild-Couder Telescope," in [*Optical System Alignment, Tolerancing, and Verification XIII*], Sasián, J. and Youngworth, R. N., eds., **11488**, 10 – 28, International Society for Optics and Photonics, SPIE (2020).

[7] [*Contributions of the Cherenkov Telescope Array (CTA) to the 6th International Symposium on High-Energy Gamma-Ray Astronomy (Gamma 2016)*] (10 2016).